SPE-182635-MS

Flow Diagnostics on Fully Unstructured Grids

Zhao Zhang and Sebastian Geiger, Heriot-Watt University; Margaret Rood, Carl Jacquemyn, Matthew Jackson, and Gary Hampson, Imperial College London; Felipe Moura De Carvalho, Clarissa Coda Marques Machado Silva, Julio Machado Silva, and Mario Costa Sousa, University of Calgary

This paper was prepared for presentation at the SPE Reservoir Simulation Conference held in Montgomery, TX, USA, 20–22 February 2017.

Abstract

Flow-diagnostics are a common way to rank and cluster ensembles of reservoir models based on their approximate dynamic behaviour prior to commencing full-physics reservoir simulation. Traditionally, flow diagnostics are carried out on corner-point grids inherent to geocellular models.

The novel "Rapid Reservoir Modelling" (RRM) concept enables fast and intuitive prototyping and updating of reservoir models. In RRM, complex reservoir heterogeneities are modelled as discrete volumes bounded by surfaces that can be modified using simple sketching operations in real time. The resulting reservoir models are discretized using fully unstructured 3D meshes where the grid conforms to the reservoir geometry.

This paper presents a new and computationally efficient numerical scheme that enables flow diagnostic calculations on fully unstructured grids. Time-of-flight and steady-state tracer distributions are computed directly on the grid. The results of these computations allows us to estimate swept reservoir volumes, injector-producer pairs, well-allocation factors, flow capacity, storage capacity and dynamic Lorenz coefficients which all help approximate the dynamic reservoir behaviour.

We use the Control Volume Finite Element Method (CVFEM) to solve the elliptic pressure equation. A scalable matrix solver (SAMG) is used to invert the linear system. A new edge-based CVFEM is developed to solve hyperbolic transport equations for time-of-flight and tracer distributions. An optimal reordering technique is employed to deal with each control volume locally such that the hyperbolic equations can be computed in an efficient node-by-node manner. This reordering algorithm scales linearly with the number of unknowns.

The total CPU time, including grid generation and flow diagnostics, is typically below 3 seconds for grids with 50k unknowns. Such fast calculations provide, for the first time, real-time feedback on changes in the dynamic reservoir behaviour while the reservoir model is updated.

Introduction

Geological heterogeneities in hydrocarbon reservoirs are multi-scale in nature and the spatial distribution of these heterogeneities, and associated petrophysical properties, is uncertain. Conventional and commercially available workflows are often too time-consuming to explore how such uncertainty impacts on hydrocarbon-

in-place estimates and predictions of future production, especially early during development when economic uncertainties are greatest. It is hence common practice to lock in geological concepts early and anchor development strategies around a single "base case" rather than exploring geological uncertainties over a range of models (Bentley, 2015). Changing this base case later on to explore further scenarios is too time-consuming and impractical. Yet, focusing too early on a single geological concept when building static and dynamic reservoir models leads to significant underestimation of uncertainties, because the same geological data can be interpreted in several different ways. The use of multiple geological concepts may lead to vastly different predictions of hydrocarbon-in-place volumes and distributions (e.g., Rankey and Mitchell, 2003; Bond et al., 2007), which will require different decisions about optimal reservoir development over the life of a field (e.g. Arnold et al. 2016).

To overcome this challenge, Jackson et al. (2015a) have recently introduced the concept of Rapid Reservoir Modelling (RRM), where the same data can be interpreted by creating prototype models based on different geological concepts, using intuitive and geologically consistent sketching operations to explore reservoir model uncertainty (Figure 1). One of the enabling technologies behind RRM is the computer graphics field of sketch-based interfaces and modeling (SBIM) (Olsen et al., 2009). SBIM techniques process user input drawings from practitioners to be used in three interrelated ways: (1) to define the geometries and topologies of 3D digital models from available geological data (if any); (2) to augment existing digital models by adding geometric details; and (3) to define user interface operations. The SBIM paradigm enables a more natural, faster, interactive and interpretive construction of 3D models. The resulting reservoir geometry is modelled as discrete volumes representing the geological heterogeneities. Unstructured meshes are hence needed to represent the resulting, geometrically complex geometries more accurately by respecting the bounding surfaces, and to refine the mesh smoothly and efficiently as needed. Delaunay-based unstructured tetrahedral meshes provide an efficient and robust to create suitable meshes for such complex 3D geometries (e.g., Milliotte and Matthai, 2014; Si, 2015; Jackson et al., 2015b). In RRM we have incorporated the Delaunay-based unstructured grid tetrahedral generator TetGen (Si, 2015).

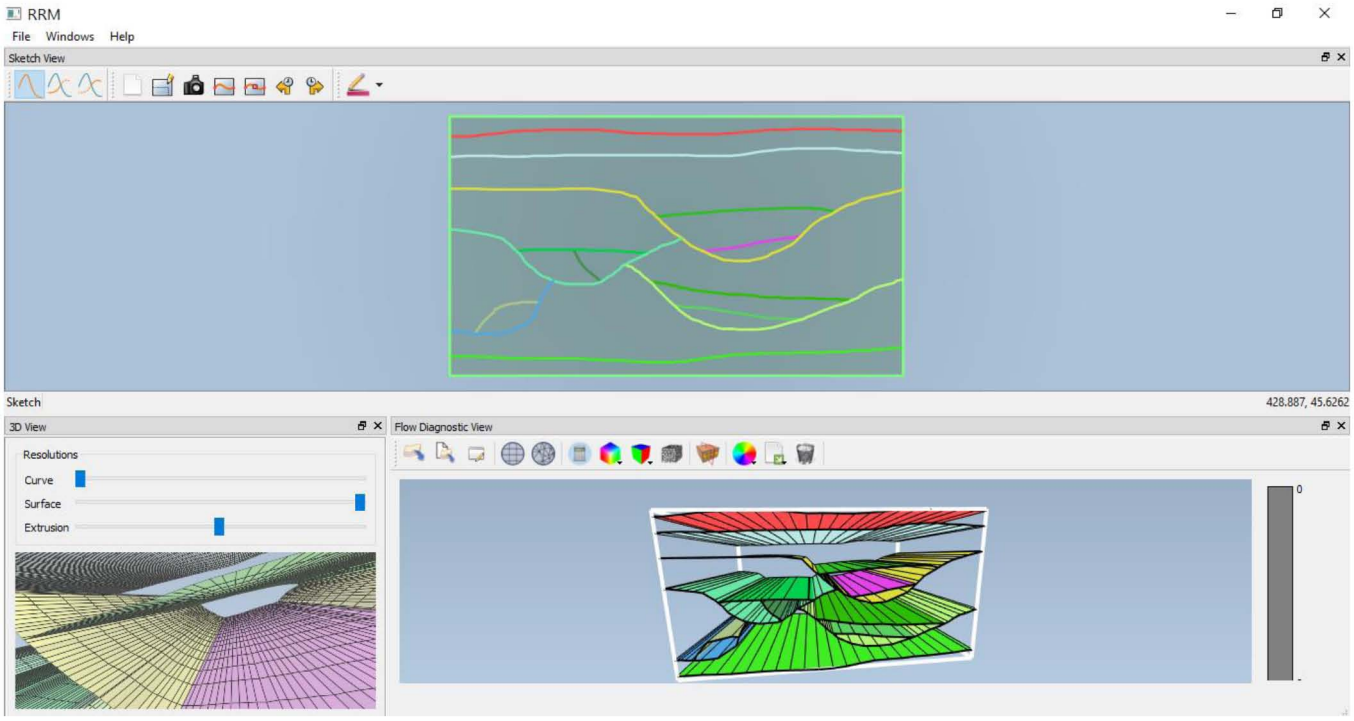

Figure 1—Screenshot of the RRM prototype showing a sketching window (top) where horizons interpreted on different seismic lines or other data can be sketched, and from which a 3D model is generated in real time (bottom right window).

However, it is prohibitively expensive to run full-physics (e.g. Black-Oil or compositional) simulations for these grids (e.g. Geiger et al., 2009). Other, more computationally efficient approaches are therefore needed to in order to compare and rank the different models and their underlying concepts, both in terms of their static and (quasi-)dynamic properties. Streamlines can be readily computed for fast flow calculations by integrating the velocity field and streamline-based simulation methods have been employed to offer flow diagnostic information (Datta-Gupta and King, 2007). While streamlines are efficient for nearly orthogonal structured grids (e.g. Thiele et al., 2003; Batycky et al., 2005), care is needed for general corner-point grids (Shahvali et al., 2012) and computational challenges arise when applying streamlines to generalised unstructured meshes (e.g., Matringe et al., 2007; Hægland, 2009; Rasmussen, 2010).

Shahvali et al. (2012) introduced an alternative to derive flow diagnostic information based on the solutions of advective transport equations for time-of-flight (TOF) and tracer calculations using a cell-centred finite volume method. Møyner et al. (2015) applied this approach to corner-point grid based models for geological modelling as well as field development planning. In particular, they adopt a technique by Natvig et al. (2007) to reorder the unknowns for fast computation.

In this paper we extend the approach of Natvig et al. (2007) and Møyner et al. (2015) by applying it to generalized unstructured grids that are suitable for the RRM framework. We present a new edge-based Control Volume Finite Element Method (CVFEM) for the advective transport equaitons and flow diagnostics on general unstructured meshes. This new approach combines the merits of CVFEM and edge-based data structure. It can be applied on any type of mesh, and particularly is suitable for 3D unstructured meshes. CVFEM benefits from both the accuracy of finite element methods and the inherent mass conservation of finite volume methods. Edge-based data structure offers a convenient way of discretisation and can be employed on any type of structured, unstructured or hybrid meshes. It is preferred for efficient computation and has been adopted in various engineering and environmental projects and applications (Lyra et al., 2004; Sun et al., 2010; Al Qubeissi, 2013; Zhang, 2015; Szmelter et al., 2015; Smolarkiewicz et al., 2016). The optimal reordering technique of Natvig et al. (2007) is adopted to unstructured grids to reduce the computational cost by dealing with each control volume locally, and the edge-based CVFEM formulation proves to be ideal for the reordering process.

Governing Equations

For ease of illustration, we consider steady-state single-phase incompressible flow governed by Darcy's law and mass conservation but note that the extension to multiphase flow is straightforward. The governing equations are

$$v = -\frac{\boldsymbol{K}}{\mu}\nabla p, \tag{1}$$

$$\nabla \cdot v = f, \tag{2}$$

where p is corrected pressure that equals to P - ρqz and v is the Darcy velocity. P is absolute pressure, ρ is density, g is gravitational acceleration, $\boldsymbol{K}$ is the permeability tensor, μ is the dynamic viscosity of the fluid and f is a source or sink term. (1) and (2) yield the standard elliptic pressure equation

$$-\nabla \cdot \left(\frac{\boldsymbol{K}}{\mu}\nabla p\right) = f. \tag{3}$$

The corrected pressure p in the reservoir can be computed from Equation (3) subject to the appropriate boundary conditions. Once the pressure field is known, Equation (1) is used to compute the velocity field, which is the basis for subsequent TOF and tracer calculations.

Following Natvig et al. (2007), the stationary transport equations for TOF and tracer calculations in Eulerian coordinates have the following hyperbolic form

$$v \cdot \nabla\tau = \varphi, \tag{4}$$

$$v \cdot \nabla c = 0, \tag{5}$$

where τ is TOF, c is the tracer, and φ stands for porosity. Assuming that the discretization method for Equation (2) is mass conservative, Equations (4) and (5) can be rewritten in the following form to help numerical discretization

$$\nabla \cdot (v\tau) = \varphi, \tag{6}$$

$$\nabla \cdot (vc) = 0. \tag{7}$$

The TOF values provide the approximate travel times between injector and producer pairs in a reservoir, in the same way as streamline simulations do, but are now calculated directly on the grid. Tracers provide additional flow diagnostics and can be used to locate the swept areas in a reservoir, estimate drainage volumes, or identify regions associated with specific injector-producer pairs (Moyner et al., 2015). Further useful flow diagnostics such as dynamic flow capacity curves can also be computed from TOF and tracer distributions (Shook, 2009)

Edge-Based Control Volume Finite Element Method

Our discretization scheme for the elliptic Equation (3) uses the well-known Control Volume Finite Element Method (CVFEM) that was first introduced by Baliga and Patankar (1980). A description of CVFEM descretizaion on 3D unstructured meshes can be found in Mello et al. (2009). The model domain is partitioned into a collection of non-overlapping polyhedral elements, termed the "finite element mesh". Then the corresponding dual mesh is constructed for CVFEM, termed the "control volume mesh". In 2D, the control volume surrounding a node of the finite element mesh is created by joining the centroids of the neighbouring polygons and the edge midpoints. In 3D, the control volume is constructed by connecting the centroids of tetrahedra, their faces and the mid-points of their edges. The correspondence between control volumes and nodes is one-to-one. Figure 2 illustrates the construction of CVFEMs in 2D and 3D.

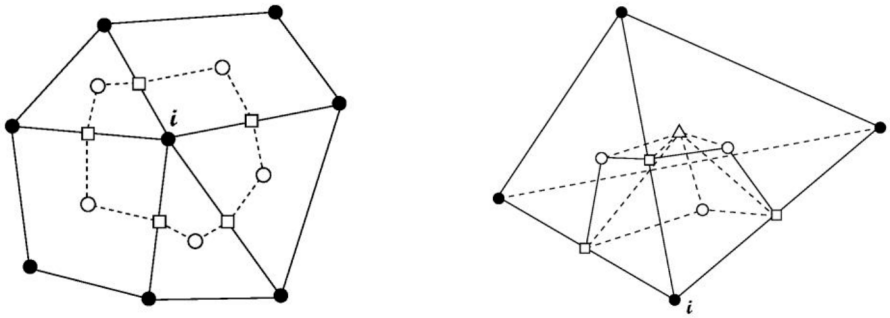

Figure 2—Illustration of the control volume construction in 2D (left) and 3D (right) from finite element meshes in the CVFEM method. Solid nodes belong to the primary finite element mesh, small circles are centroids of polygons, small squares are edge midpoints, and small triangles represent tetrahedron centroids. In 2D, each polygon surrounding node i contains two segments of the control volume boundary. The control volume of node i is built by connecting all these segments. In 3D, in the case of a tetrahedral mesh, each tetrahedron surrounding node i contributes six triangular bounding faces for the control volume. The figure shows one of the tetrahedrons. Each triangular bounding face is formed by connecting the centroid of the tetrahedron, a face centroid and an edge midpoint. The control volume of node i in 3D is built by connecting all these bounding faces.

Let i be an integer denoting the node number and Ω_i be the control volume containing the node. To obtain a linear system to solve for the corrected pressure p, Equation (3)) is integrated over each control volume and the Divergence theorem is applied

$$\int_{\partial\Omega_i} \vec{n} \cdot (\frac{K}{\mu} \nabla p) dS = \int_{\Omega_i} f dV, \tag{8}$$

Properties $\boldsymbol{K}$ and μ are both defined on the elements while p is defined on the nodes and interpolated on the finite element mesh using piecewise linear basis functions. The linear equation system for p from Equation (8)) can be solved efficiently by the Algebraic Multigrid (AMG) method (Stüben, 2007), for which we use the library SAMG. From the solution of the pressure field, piece-wise constant Darcy velocity can be readily computed from Equation (1)) on the finite elements. The transport Equations (6) and (7) for TOF and tracer calculations, respectively, have the same hypobolic form

$$\nabla \cdot (\, vu) = b, \tag{9}$$

where u is TOF or tracer and b is the corresponding source term. Integration over each control volume and application of the Divergence theorem yields

$$\int_{\partial\Omega_i} u\vec{v} \cdot \vec{n}\, dS = \int_{\Omega_i} b dV. \tag{10}$$

For a 3D unstructured mesh, the control volume of node i is bounded by triangular faces, and node i is connected to its neighbouring nodes by edges. We employ an edge-based data structure (see Figure 3) and approximate Equation (10)) by

$$\sum_{j \in E_i} u_{ij} q_{ij} = b_i V_i, \tag{11}$$

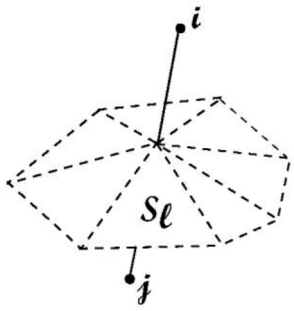

Figure 3—Illustration of the edge-based data structure. The triangular bounding faces of node *i* or *j* are grouped together to form this "small umbrella", which also comprises the shared faces of the two control volumes of node *i* and *j*. Sl is one of the triangular bounding faces of the control volume of node *i* or *j*.

where E_i is the set of all neighbouring nodes of node i, and u_{ij} is the value of u at the midpoint of edge ij connecting nodes i and j. Assuming b is constant in Ω_i with volume V_i, the right-hand-side term becomes $b_i V_i$. Given b is defined on elements, b_i is approximated by the weighted average from all neighboring elements.

The total flux through faces connecting to edge ij is

$$q_{ij} = \sum_{l \in E_i} \overrightarrow{v_k} \cdot \overrightarrow{n_l} A_l, \tag{12}$$

where C is the set of all triangular faces S_l from the midpoint of edge ij. The unit normal vector pointing outwards and the area of S_l are denoted as $\overrightarrow{n_l}$ and A_l, respectively. $\overrightarrow{v_k}$ is the velocity of the element that contains S_l. The definition of q_{ij} is essentially a multi-point approximation, and is consistent with the formulation of CVFEM that mass conservation is preserved. However, CVFEM can lead to numerical errors in the case of strong permeability anisotropy, which can be corrected at extra computational cost (Edwards, 2006). Let u be defined on the nodes, the edge value u_{ij} is approximated by the upwind value based on the higher flow potential P - ρqz.

Reordering Based on Depth First Search

We use the optimal reordering strategy of Natvig et al. (2007) to solve Equation (11)) locally for each control volume. The reordering technique is based on a depth-first search (DFS). The first step is to build a directed topological graph, where the control volume for each node is represented by a vertex, while a directed edge is built between a vertex and each of its neighbours. The edges always point from nodes of higher flow potential P - ρqz to those with lower potential, consistent with the upwind scheme.

Performing DFS on the graph produces a sequence of nodes if the graph is acyclic. Then Equation (11)) is solved locally node-by-node according to the sequence, with values of all upstream nodes already known. If such a sequence does not exist, the graph contains cycles. A cycle is detected in DFS when a vertex is searched more than once. The values of the vertices in a cycle need to be computed simultaneously since they are interdependent, which makes the computation more intensive.

In RRM, there is one boundary condition for TOF and one for each of the tracers. These boundary conditions are defined at the wells. Since each vertex is either searched just once or not visited at all by DFS, the number of operations needed for the topological sorting is $O(N_d N_b)$, where N_d is the average number of nodes downstream of TOF and tracer boundaries, and N_b the number of boundaries. For an acyclic graph, the computational cost for solving Equation (11)) locally after reordering scales linearly with the number of unknowns (Natvig et al., 2007; Natvig and Lie, 2008). For our upwind scheme, we can make sure that the corresponding graph is acyclic, regardless of mesh quality. To prove this, suppose there is a cycle of size n, which is

$$i_1 \rightarrow i_2 \rightarrow i_3 \rightarrow \ldots\ldots \rightarrow i_n \rightarrow i_1, \tag{13}$$

where $i_1,\ldots\ldots,i_n$ are nodes in the cycle. Then the nodes' corrected pressures satisfy

$$p_1 > p_2 > p_3 > \ldots\ldots > p_n > p_1, \tag{14}$$

which is in contradiction. Therefore, the graph contains no cycles.

Derived Quantities for Flow Diagnostics

Quantitative flow diagnostics information can be derived from the TOF and tracer distributions (Shook, 2009; Shahvali et al., 2012; Møyner et al., 2015). Well-pair pore volume and well allocation factors are computed based on tracers. Our method is similar to that of Shahvali et al. (2012), but with variables defined on nodes of a generalized unstructured grid. The average value of a variable on each control volume is represented by the corresponding nodal value. Let c_k^i be the tracer value of node k for well i, representing the fraction of control volume k for well i. Then $c_{ij} = c_i c_j$ is the fraction for injection-producer pair ij. The well-pair pore volume is given by

$$V^{ij} = \sum_{k \in M} V_k^{ij} = \sum_{k \in M} c_k^{ij} \varphi_k V_k \tag{15}$$

where M is the set of all nodes in the mesh. φ_k and V_k are the porosity and volume of control volume k, respectively. V_k^{ij} is the pore volume of control volume k associated with well pair ij. The well allocation factor is the flux associated with the well pair. The total influx and outflux of control volume k are denoted as q_k^{in} and q_k^{out}, respectively, and are computed as

$$q_k^{in} = -\sum_{j \in E_k} \min(q_{kj}, 0) \tag{16}$$

$$q_k^{out} = \sum_{j \in E_k} \max(q_{kj}, 0) \tag{17}$$

The total influx and outflux associated with well pair ij are given by

$$Q_{ij}^{in} = \sum_{k\in M} c_k^{ij} q_k^{in} \tag{18}$$

$$Q_{ij}^{out} = \sum_{k\in M} c_k^{ij} q_k^{out} \tag{19}$$

Because of mass conservation, we have $q_k^{in} = q_k^{out}$ and $Q_{ij}^{in} = Q_{ij}^{out}$. The well allocation factor is

$$W_{ij} = \frac{Q_{ij}^{in}}{\sum_{k\in M} q_k^{in}} \tag{20}$$

Flow-capacity/storage-capacity diagrams and Lorenz coefficients can be computed based on TOF for assessing heterogeneity. TOF computed from Equation (6)) is also called forward TOF, the time it takes for a fluid particle to arrive at its current location after it was injected at a given well. If we reverse the flow field and treat the producers as inlet boundaries, the computed TOF would be the backward TOF which is the time a fluid particle will take to reach a given producer from its current location. We denote the forward TOF of node *k* as τ_k^f and the backward TOF as τ_k^b, then the total travel time is $\tau_k^{total} = \tau_k^f + \tau_k^b$. The average volumetric rate for node *k* and well pair *ij* is computed as

$$f_k^{ij} = V_k^{ij} / \tau_k^{total}. \tag{21}$$

All nodes are sorted according to ascending τ_k^{total}. Suppose there are *n* nodes in total, the flow capacity and storage capacity for each well pair are defined as

$$F_m^{ij} = \sum_{k=1}^{m} f_k^{ij} / \sum_{k=1}^{n} f_k^{ij} \quad \text{and} \quad \Phi_m^{ij} = \sum_{k=1}^{m} V_k^{ij} / \sum_{k=1}^{n} V_k^{ij}. \tag{22}$$

The corresponding dynamic Lorenz coefficient is defined as (Shook, 2009)

$$Lc^{ij} = \sum_{m=1}^{n} \left(F_m^{ij} + F_{m-1}^{ij}\right)\left(\Phi_m^{ij} - \Phi_{m-1}^{ij}\right) - 1, \tag{23}$$

assuming

$F_0^{ij} = \Phi_0^{ij} = 0$. The flow-capacity/storage-capacity curve for a homogeneous displacement is a straight line with slope one and corresponding Lorenz coefficient zero.

Validation using a Homogeneous 5-spot Example

We demonstrate the validation and computational efficieny of our unstructured flow diagnostics method using a 5-spot example. The reservoir model is a 1000 m × 1000 m × 200 m cuboid with homogeneous permeability 500 mD and porosity 0.2. An injector is placed in the centre of the model with four producers at the four corners. All wells are vertical, penetrate the entire formation and are pressure controlled. The injector and producers have corrected pressure 100 and 1 bar, respectively, and all other boundaries have no-flow condition. There are no other sources or sinks. The flow is assumed to be single-phase and incompressible with viscosity 1 cP. The objective of this test case is to validate the numerical methods via a symmetrical model. Here we use ParaView to visualize the results but note that the visualization is done automatically in RRM. The fully unstructured tetrahedral mesh is generated by calling to TetGen as an internal library in RRM (Figure 4). The number of elements and nodes is 50779 and 9579, respectively. For generating a quality mesh using TetGen, the maximum allowable radius-edge ratio is set to be 1.0, and the minimum allowable dihedral angle is set to be 30 degrees. The radius-edge ratio of a tetrahedron is the ratio of circumscribed sphere radius to smallest edge length (Miller et al., 1999). The mesh respects the wells which are represented as lines of nodes. Corrected pressures (Figure 4a) and elemental velocities

are computed by CVFEM, and subsequently forward and backward TOF and tracer values for nodes are calculated by the edge-based CVFEM, volume-by-volume locally after reordering.

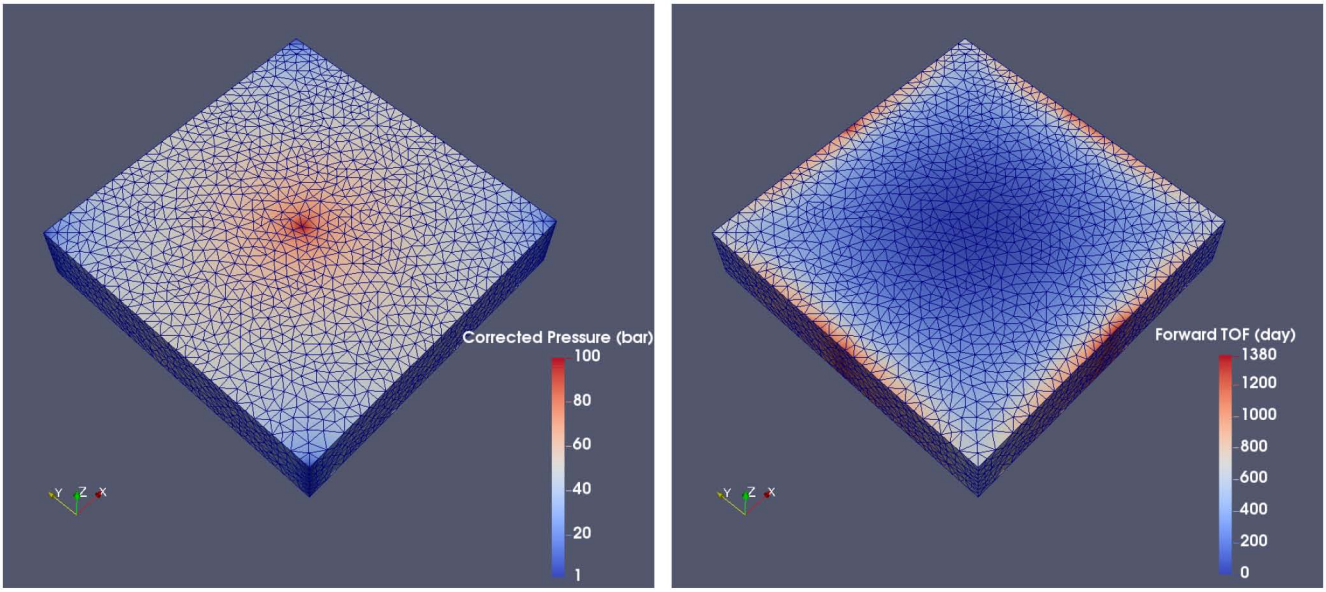

Figure 4—Corrected pressure field calculated on the nodes (a) and corresponding forward TOF (b) for a 5-spot model with uniform permeability and porosity (domain size 1000 m × 1000 m × 200 m).

The corresponding Forward TOF values are shown in Figure 4b. Since there is only one injector, the reservoir is partitioned based on on the four producers, resulting in four symmetrical and equally-sized quadrants, each having 25% of the total pore volume. To validate that these quadrants are detected correctly and automatically in our flow diagnostics, each producer is associated with a unique tracer. Equation (7)) is solved for each tracer with the concentration set to unity at the corresponding producer. The flow field is reversed for the tracer computation. This is done by reversing q_{ij} associated with the edges. Each node has four tracer values, and is assigned to a producer via a majority vote, such that the reservoir can be partitioned into different injector-producer regions. Figure 5a shows the resulting reservoir partitioning based on majority vote for all four tracers, which is approximately symmetrical and equally sized despite the unstructured mesh. Figure 5b shows the partitioning on a coarser mesh. The comparison shows that higher mesh resolution leads to more accurate reservoir partitioning. Well-pair pore volumes and well allocation factors can also be computed based on tracer values. Figure 6 shows the pore volume for all well pairs and the solution is accurate within a relative standard deviation of 0.33%. Figure 6 also shows the well allocation factors for the well pairs, which are calculated correctly within a relative standard deviation of 0.65%. The deviation is partially due to the fact that the mesh is inevitably not generated exactly along the boundary of the partition. The relative standard deviation stays below 2% for meshes with more than 8k elements and below 1.5% for meshes with more than 100k elements.

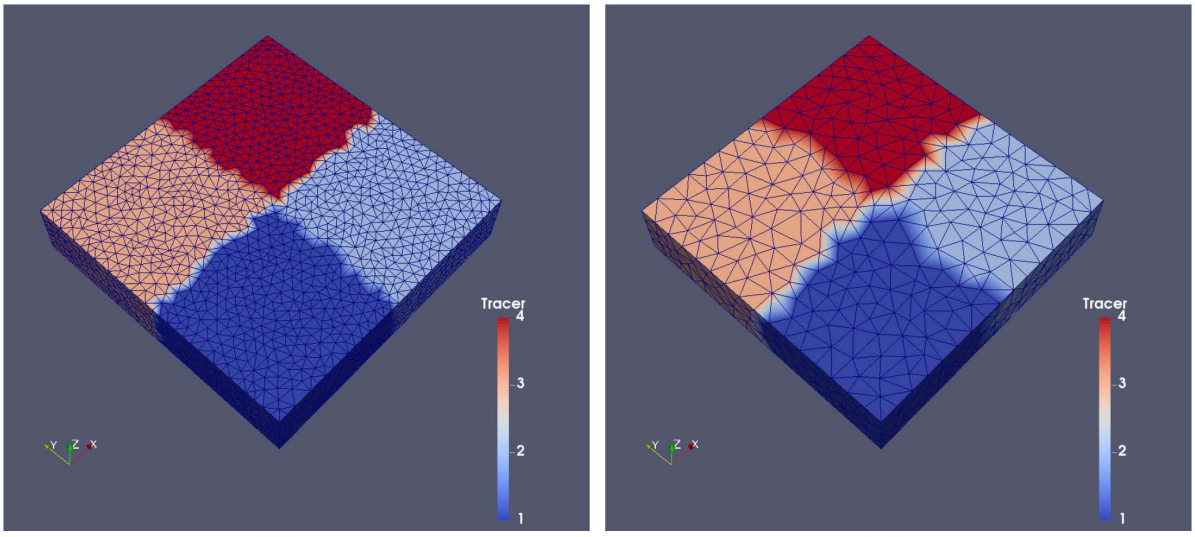

(a) (b)

Figure 5—Reservoir injector-producer partitioning for the entire reservoir in the 5-spot example (a). The partition is approximately symmetric despite the unstructured mesh. The partitioning obtained using a much coarser mesh is also shown for comparison (b).

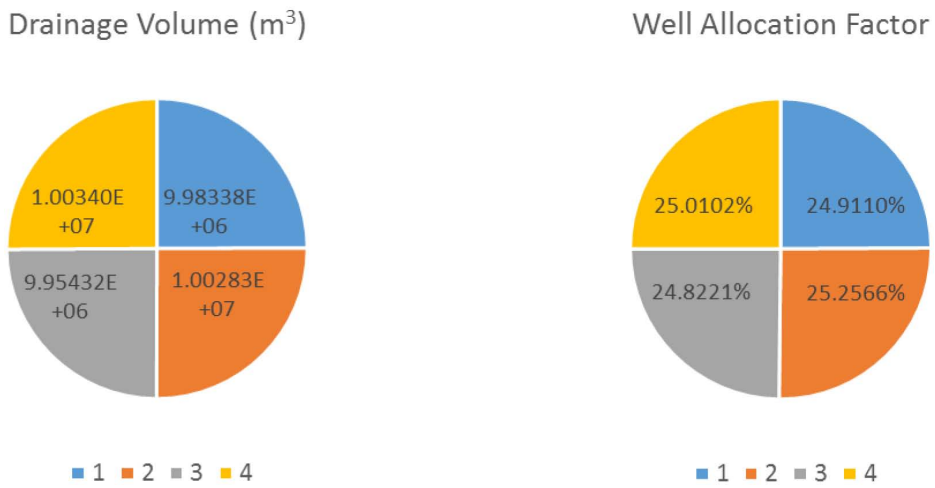

Figure 6—Pore volumes (left) and allocation factors (right) associated with the four different injector-producer pairs in the 5-spot example. Since the model is symmetrical and properties are uniform, the allocation factor for each well pair should be 25% and each pore volume should comprise 25% of the entire reservoir pore volume (i.e., 10^7 m^3).

It is important to note the total CPU time required for the whole calculation. In this example, these calculations include unstructured meshing, and computing for pressure, velocity, forward and backward TOF, four tracer distributions and tracer-based derived quantities. We have implemented the algorithms in C++ and less than 1.5 seconds is required to perform all calculations on a HP Z230 workstation with an Intel® Core™ i7-4790 CPU with 3.60GHZ and 64-bit Windows 7 operating system. The same procedure is repeated for different mesh resolutions. The total CPU time and average time per element are shown in Figure 7. The average CPU time per element first drops considerabaly and then stays approximately constant as the mesh is refined. The reason is that the parts of the code that are not related to loops of elements/nodes require similar CPU time for different meshes. Thus the CPU time per element first decreases with increasing number of elements until the cost for these operations becomes very small compared to the cost of calculations that are required to loop over elements and nodes. Once these calculations begin to dominate, the CPU time is $O(N)$ where N is the number of elements or nodes.

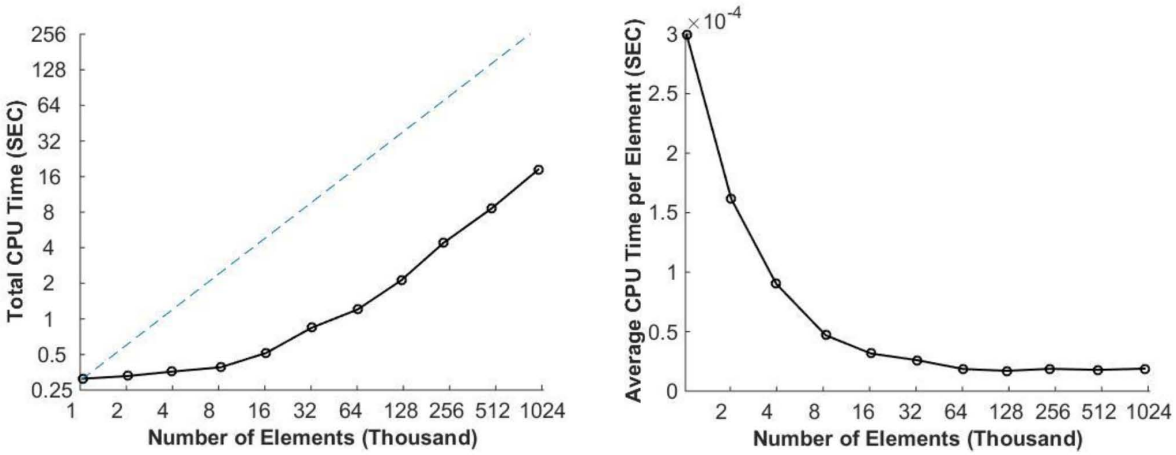

Figure 7—Total CPU time for different levels of mesh refinement applied to the 5-spot example (left). Note that both axes are LOG_2 scaled. The dashed reference line has a slope of one. The corresponding average CPU time per element for different meshes, where only the x-axis is LOG_2 scaled (right).

Example using Channelised Sandbodies

To demonstrate that our calculations can be applied to more realistic geological structures, we perform flow diagnostics on an unstructured grid that represents a series of stacked channelised sandbodies (e.g. in a fluvial or deepwater reservoir). The dimensions of the model are $x_{max} = 100.63m$, $x_{min} = -1083.44$ m, $Y_{max} = 944.26$ m, $Y_{min} = 71.43$ m, $z_{max} = 180.00$ m and $z_{min} = 10.00$ m. The channelised sandbodies are marked by different colours and meshed using unstructured tetrahedrons (Figure 8a). Clearly, it would be very challenging if not impossible to represent this geometry adequately using structured Cartesian or corner point grids. There are 12854 tetrahedral elements and 3905 nodes in the mesh. The inlet and outlet boundaries for the model have fixed pressure boundary condition $p(x)$ given by

$$p(x) = \begin{cases} 500 - 0.1(x - x_{min}) \text{ (bar) for inlet} \\ 2 + 0.1(x_{max} - x) \text{ (bar) for outlet} \end{cases} \quad (24)$$

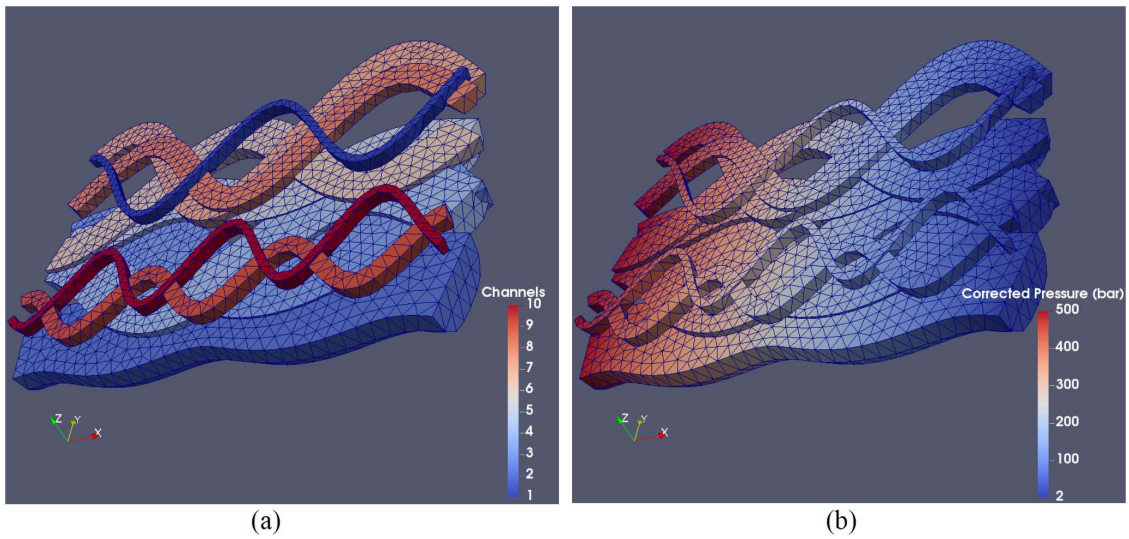

(a) (b)

Figure 8—Ten channelised sandbodies with differend petrophysical properties (Table 1) represented by an unstructured tetrahedral mesh courtesy of Y. Melnikova, Imperial College London (a). The channelised sandbodies are marked by different colours. The number of elements and nodes is 12854 and 3905, respectively. Distribution of corrected pressure (b).

while all other boundaries have no-flow conditions. Table 1 summarises the petrophysical properties of the channelised sandbodies. The flow is assumed to be single-phase and incompressible with viscosity 1 cP and isotropic permeabilities.

Table 1—Porosity and permeability for the channelised sandbodies

Channel ID	Porosity	Permeability (mD)
1, 2, 3, 4	0.2	100
5, 6, 7, 8	0.2	200
9, 10	0.2	1000

Figure 8b shows the distribution of the corrected pressure p while Figure 9a depdicts the forward TOF plot and Figure 9b shows the total travel time.

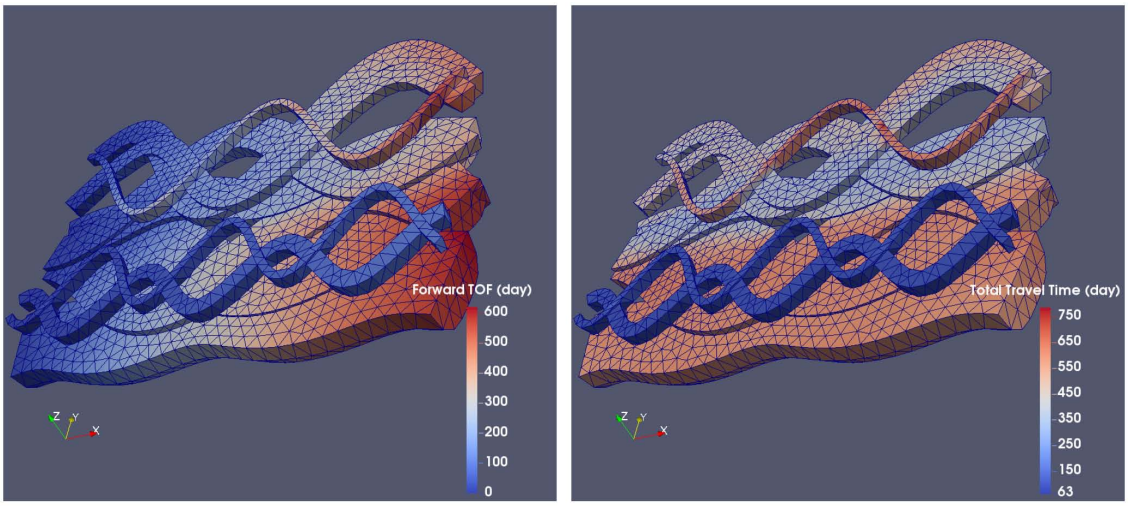

(a) (b)

Figure 9—Foward TOF in ten channelised sandbodies (a) and total travel time (b) in the same channelised sandbodies. See Table 1 and Figure 8 for the petrophysical properties of the sandbodies.

Since the permeability in each channelised sandbody is isotropic and constant, the total travel time is approximately constant for each channelised sandbody, except in areas where sandbodies cross each other and cross-flow occurs between them. Since there is only one inflow and one outflow boundary, tracer calculations are not needed. Next, we assume homogeneous rock properties for the whole model and repeat the computation. The isotropic permeability value is 200 mD and the porosity is 0.2 for the homogeneous properties case. Flow capacity and storage capacity for both cases are computed based on Equation (22)) and shown in Figure 10. The correcponding Lorenz coefficients for the cases of heterogeneous and homogeneous properties are 0.222 and 0.062, respectively. The CPU time for the process of reading in the finite element mesh, building the control volume data structure, computing steady-state solution and flow diagnostics of the heterogeneous case is less than 0.7 sec using the same hardware as in the 5-spot example. Note that for computing flow and storage capacity, the nodes need to be sorted according to ascending total travel time. The sorting of nodes can be $O(nlog_2n)$ or $O(n^2)$, where n is the number of nodes, depending on the algorithm adopted (Cormen, 2009).

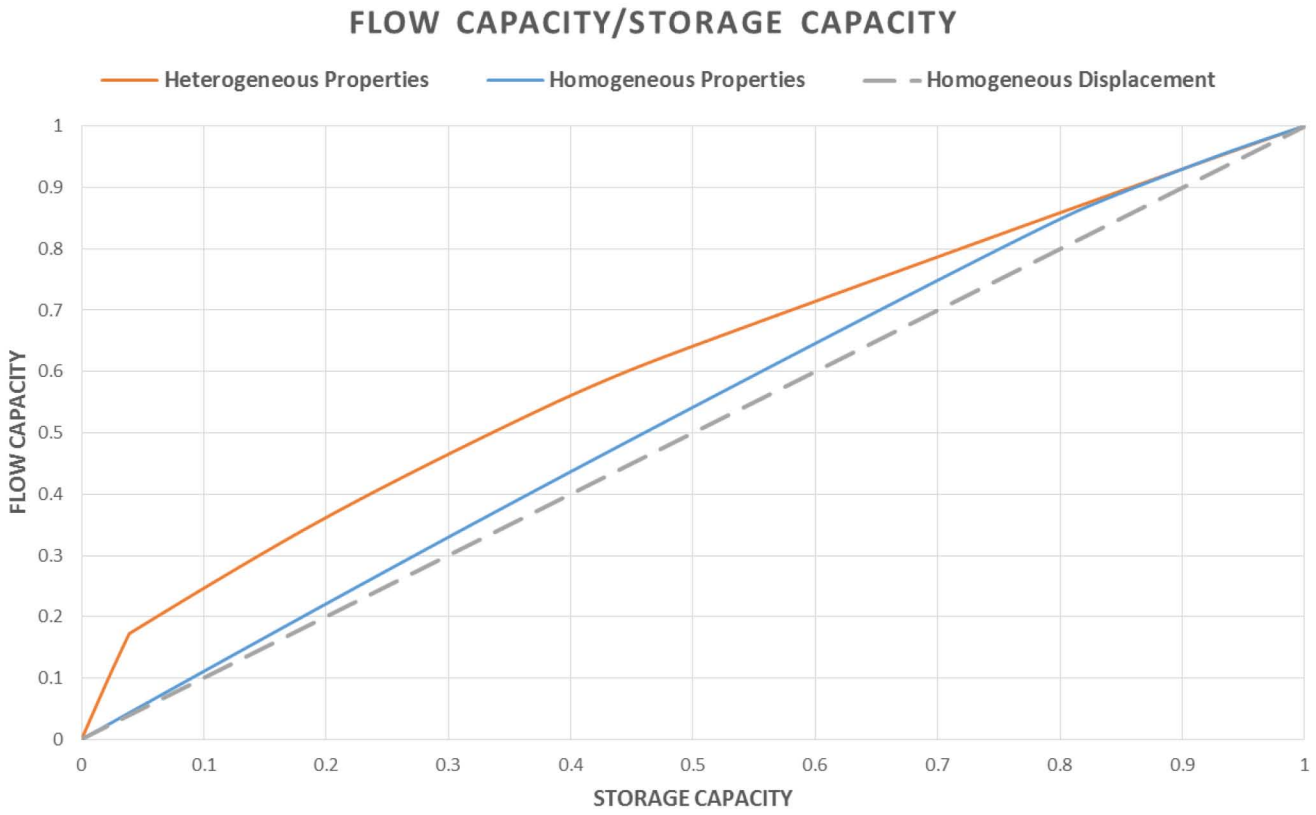

Figure 10—Flow capacity/storage capacity diagram for the heterogeneous channelised sandbodies depicted in Figures 8 and 9 (red line). The curve for homogeneous channelised sandbodies is shown in blue. The gray dashed line represents a homogeneous displacement.

RRM Example of Channelised Sediment Bodies

In RRM, sketch-based interface modelling is employed to create surfaces that define the geological model. Figure 1 shows a model of channelised sediment bodies which erode into each other, and in which each channelised body contains additional surfaces that describe the channel-infill sediments. The model is created by linear extrusion after sketching on a vertical cross-section. To obtain a water-tight triangular surface mesh from which the tetrahedral volume mesh can be created, we first convert the surfaces that are generated during the RRM sketching into parametric surfaces; this step is done automatically. There are 34216 tetrahedral elements and 6854 nodes in the volume mesh. The surfaces separate the model into 13 regions. Table 2 summarises the petrophysical properties of the regions. A constant viscosity of 1 cp is assumed for the entire model. Figure 11a shows the regions.

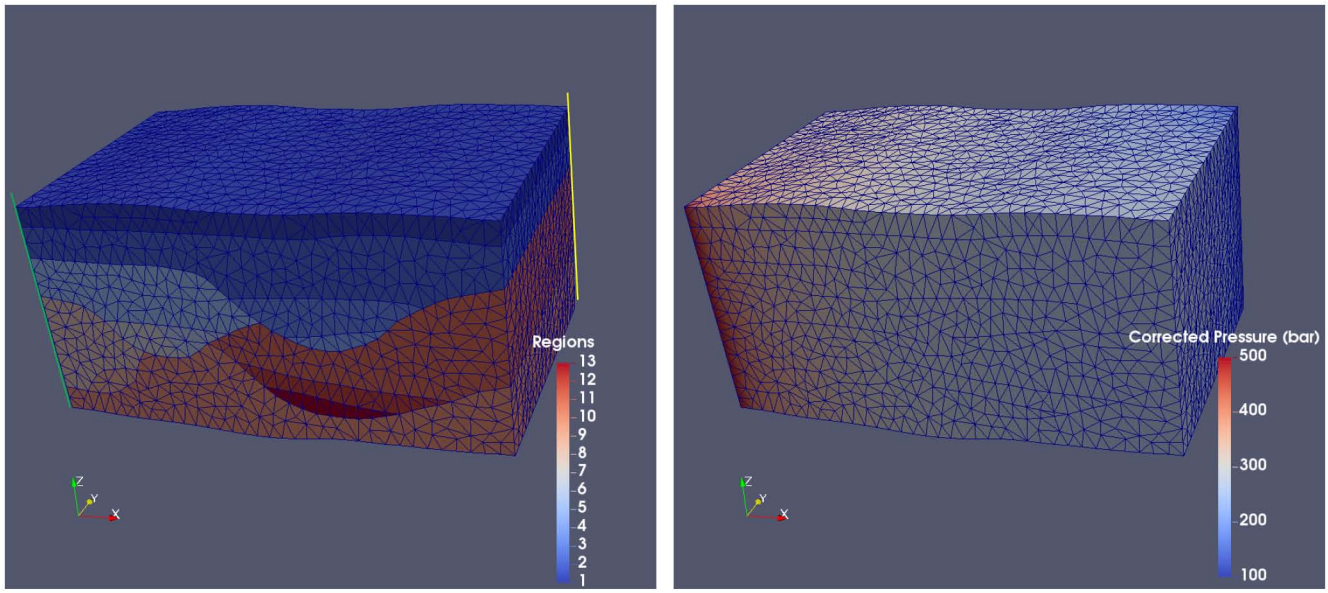

Figure 11—Permeability field for the RRM example (a). The green and yellow lines mark the position of the injector and producer, repectively. Corrected pressure field for the RRM example (b).

Table 2—Porosity and permeability values for different regions in the RRM example

Region ID	Porosity	Permeability (mD)
1	0.35	500
2	0.3	450
3	0.3	400
4	0.3	380
5	0.3	300
6	0.3	200
7	0.2	200
8	0.2	150
9	0.2	100
10	0.2	50
11	0.2	300
12	0.2	150
13	0.2	100

One injector (green) and one producer (yellow) are situated in two opposite corners of the model (Figure 11a) and penetrate the entire formation. The injector and producer operate at fixed pressures, having a corrected pressure of 500 and 100 bar, respectively. All other boundaries are no-flow conditions. The flow is assumed to be single phase and incompressible, and the full suite of flow diagnostics is performed. Figure 11b shows the corrected pressure field, Figure 12a shows the forward TOF and Figure 12b the total travel time. The computation is then repeated for a homogeneous properties case with isotropic permeability 200 mD and porosity 0.2. Figure 13 shows the flow capacity/storage capacity diagrams for both the heterogeneous and homogeneous cases, with Lorenz coefficients 0.245 and 0.128, respectively. The CPU time for generating surface and volume meshes, steady-state computation, and flow diagnostics for the heterogeneous case is less than 1.4 seconds on the same hardware as before.

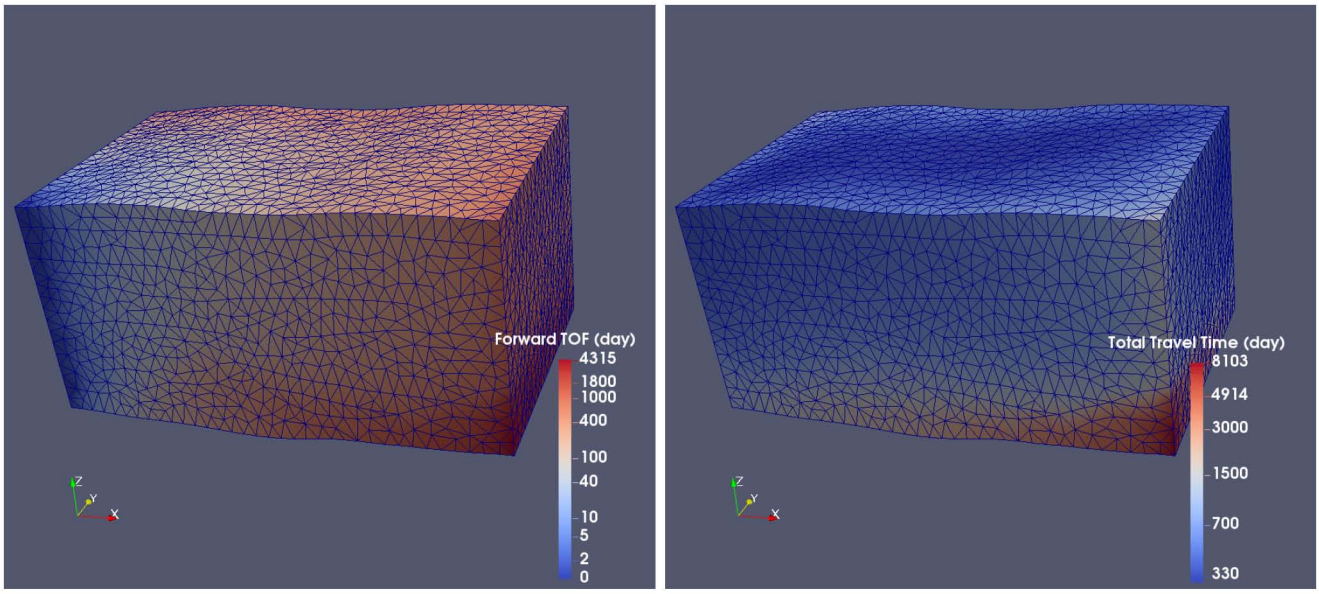

Figure 12—Forward TOF for the RRM example (a) and corresponding total travel time (b). Note that the color scheme is scaled by log_e.

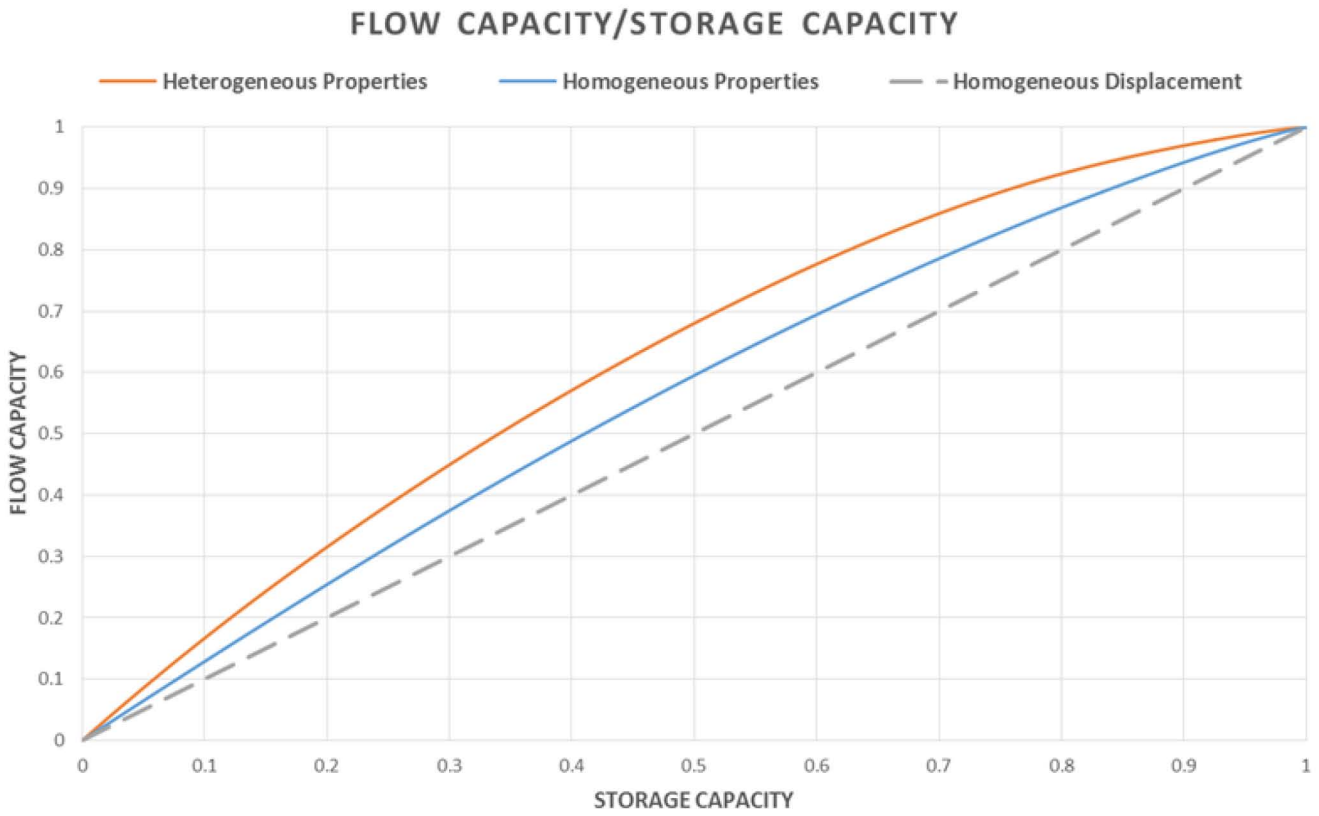

Figure 13—Flow capacity/storage capacity diagram for the RRM example. The cases with heterogeneous and homogeneous properties are plotted in red and blue, respectively. The grey dashed line represents a homogeneous displacement.

Conclusions

We have developed and validated a new edge-based Control Volume Finite Element Method (CVFEM) for flow diagnostics on fully unstructured 3D meshes to facilitate "real-time" flow diagnostics that estimate the quasi-dynamic reservoir properties when exploring different geological concepts in the Rapid Reservoir

Modelling (RRM) framework. In RRM, sketch-based interface modelling is employed to prototype reservoir models by sketching surfaces over geological data and related interpretations. Reservoir heterogeneities are modelled as discrete volumes bounded by surfaces, and 3D unstructured meshes are used for discretization when performing quantitative calculations on the resulting complex geometries.

The edge-based CVFEM formulation can be applied to any type of mesh and is particularly suitable for unstructured meshes. It benefits from the accuracy of finite element methods, the inherent mass conservation of finite volume methods and the efficiency of edge-based data structures. We present the relevant derivation for the steady-state advective transport equation, with pressure and velocity obtained using CVFEM for consistency. In addition, we have also demonstrated that the new approach is suitable for efficient local computation of tracer and time-of-flight calculations by optimally reordering the nodes using depth-first search. Based on TOF and tracers, reservoir partitioning, well-pair pore volume, well allocation factors, flow capacity/storage capacity diagrams and Lorenz coefficients can be obtained.

We have shown several applications of flow diagnostics on unstructured meshes and observed that CPU times are a few seconds at most for meshes with $O(100k)$ uknowns, allowing for real-time feedback on the quasi-dynamic flow properties as new prototypes are created that explore different reservoir concepts. Key to this computational performance is the linear scaling of the depth-first search for calculating the TOF and tracer distributions and the application of SAMG.

Acknowledgements

The members of the RRM consortium (ExxonMobil, Shell, IBM Research, Petrobras and Statoil) are gratefully thanked for funding and for granting permission to publish this work. Sebastian Geiger also thanks Foundation CMG for supporting his Chair in Carbonate Reservoir Simulation.

Bibliography

Al Qubeissi, M., *Development of a conjugate heat transfer solver*. LAP LAMBERT Academic Publishing, 2013.

Arnold, D., Demyanov, V., Christie, M., Bakay, A., Gopa, K., Optimisation of decision making under uncertainty throughout field lifetime: A fractured reservoir example. *Computers & Geosciences*, **95**, 123–139, 2016

Baliga, B., Patankar, S., A new finite-element formulation for convection-diffusion problems. *Numerical Heat Transfer* **3** (4), 393–409, 1980.

Batycky, R.P., Thiele, M.R., Baker, R.O. and Chung, S., *Revisiting reservoir flood-surveillance methods using streamlines*, SPE Paper 95402, 2005.

Bentley M., Modelling for comfort? *Petroleum Geoscience*. **22**(1):3–10, 2016

Bond C.E., Gibbs A.D., Shipton Z.K., Jones S., What do you think this is? "Conceptual uncertainty" in geoscience interpretation. *GSA Today*. **17**(11):4, 2007

Cormen, T.H., *Introduction to algorithms*. MIT press, 2009.

Datta-Gupta, A. and King, M.J., *Streamline simulation: theory and practice* (Vol. **11**). Society of Petroleum Engineers, 2007.

Edwards, M.G., Higher-resolution hyperbolic-coupled-elliptic flux-continuous CVD schemes on structured and unstructured grids in 2D. *International Journal for Numerical Methods in Fluids*. **51**:1059–1077, 2006.

Geiger, S., Matthäi, S.K., Niessner, J. and Helmig, R., Black-oil simulations for three-component, three-phase flow in fractured porous media. *SPE Journal*, **14**(02), 338–354, 2009

Hægland, H., *Streamline methods with application to flow and transport in fractured media*. Ph.D. thesis, University of Bergen, 2009.

Jackson, M., Percival, J., Mostaghimi, P., Tollit, B., Pavlidis, D., Pain, C., Blunt, M, Reservoir modeling for flow simulation by use of surfaces, adaptive unstructured meshes, and an overlapping-control-volume finite-element method. *SPE Reservoir Evaluation & Engineering*, **18**(02), 115–132, 2015b

Jackson, M., Hampson, G. J., Rood, D., Sousa, M. C., Geiger, S., Guimaraes, L.N., Rapid reservoir modelling: Prototyping of reservoir models using an intuitive, sketch-based interface. *SPE Paper 173237*, 2015a

Lyra, P., Lima, R., Guimaraes, C., de Carvalho, D., An edge-based unstructured finite volume procedure for the numerical analysis of heat conduction applications. *Journal of the Brazilian Society of Mechanical Sciences and Engineering* **26** (2), 160–169, 2004.

Matringe, S.F., Juanes, R. and Tchelepi, H.A., Tracing streamlines on unstructured grids from finite volume discretizations. *SPE Journal*, 423–431, 2008

Mello, U.T., Rodrigues, J.R.P. and Rossa, A.L., A control-volume finite-element method for three-dimensional multiphase basin modeling, *Marine and Petroleum Geology*, **26**(4), 504–518, 2009

Miller, G. L., Talmor, D., Teng, S.-H., Walkington, N., On the radius-edge condition in the control volume method. *SIAM Journal on Numerical Analysis* **36** (6), 1690–1708, 1999.

Milliotte, C., and Matthäi, S., From seismic interpretation to reservoir model: an integrated study accounting for the structural complexity of the Vienna Basin using an unstructured reservoir grid. *First Break*, **32**(5), 95–101, 2014

Møyner, O., Krogstad, S., Lie, K.-A., et al., The application of flow diagnostics for reservoir management. *SPE Journal* **20** (02), 306–323, 2015.

Natvig, J. R., Lie, K.-A., Fast computation of multiphase flow in porous media by implicit discontinuous galerkin schemes with optimal ordering of elements. *Journal of Computational Physics* **227** (24), 10108–10124, 2008.

Natvig, J. R., Lie, K.-A., Eikemo, B., Berre, I., An efficient discontinuous Galerkin method for advective transport in porous media. *Advances in water resources* **30** (12), 2424–2438, 2007.

Olsen, L., Samavati, F. F., Sousa, M. C., Jorge, J. A., Sketch-based modeling: A survey. *Computers & Graphics* **33** (1), 85–103, 2009.

Rankey E.C., Mitchell J.C., That's why it's called interpretation: Impact of horizon uncertainty on seismic attribute analysis, *The Leading Edge*, **22**(9):820–8, 2003

Rasmussen, A. F., Streamline tracing on irregular geometries. EC- MOR XII-12th European Conference on the Mathematics of Oil Recovery, Oxford, UK, 2010

Shahvali, M., Mallison, B., Wei, K., Gross, H., et al., An alternative to streamlines for flow diagnostics on structured and unstructured grids. *SPE Journal* **17** (03), 768–778, 2012.

Shook, G. M., Mitchell, K. M., et al., A robust measure of heterogeneity for ranking earth models: The F Phi curve and dynamic Lorenz coefficient. *SPE Paper 124625*, 2009

Si, H., Tetgen, a delaunay-based quality tetrahedral mesh generator. *ACM Transactions on Mathematical Software (TOMS)* **41** (2), 11, 2015.

Smolarkiewicz, P.K., Deconinck, W., Hamrud, M., Kühnlein, C., Mozdzynski, G., Szmelter, J. and Wedi, N.P., A finite-volume module for simulating global all-scale atmospheric flows. *Journal of Computational Physics*, **314**, 287–304, 2016.

Stüben, K., Clees, T., Klie, H., Lu, B. and Wheeler, M.F., Algebraic multigrid methods (AMG) for the efficient solution of fully implicit formulations in reservoir simulation. *SPE Paper 105832*, 2007

Sun, Z., Chew, J. W., Hills, N. J., Volkov, K. N., Barnes, C. J., Efficient finite element analysis/computational fl dynamics thermal coupling for engineering applications. *Journal of turbomachinery* **132** (3), 031016, 2010.

Szmelter, J., Zhang, Z., Smolarkiewicz, P. K., An unstructured-mesh atmospheric model for nonhydrostatic dynamics: Towards optimal mesh resolution. *Journal of Computational Physics* **294**, 363–381, 2015.

Thiele, M. R., Batycky, R., et al., Water injection optimization using a streamline-based workflow. *SPE Paper 84080*, 2003.

Zhang, Z., *Unstructured mesh methods for stratified turbulent flows*. Ph.D. Thesis, Loughborough University, 2015.